Effective permeability tensor and double resonance of interacting bistable ferromagnetic nanowires

Vincent Boucher,[1,*] Louis-Philippe Carignan,[1,2] Toshiro Kodera,[2] Christophe Caloz,[2] Arthur Yelon,[1] and David Ménard[1,†]
[1]*Département de Génie Physique, Regroupement Québécois sur les Matériaux de Pointe (RQMP), École Polytechnique de Montréal, CP 6079, Succ. Centre-ville, Montréal, Québec, Canada H3C 3A7*
[2]*Département de Génie Électrique, Centre de Recherche Poly-Grames and Centre de Recherche en Électronique Radiofréquence (CREER), École Polytechnique de Montréal, CP 6079, Succ. Centre-ville, Montréal, Québec, Canada H3C 3A7*
(Received 17 August 2009; published 1 December 2009)

We present a model for the effective permeability tensor of nonsaturated arrays of axially magnetized bistable ferromagnetic wires based on a Maxwell-Garnett formalism generalized to include the case of two oppositely magnetized wire populations. Explicit expressions for the complex diagonal and off-diagonal components of the effective permeability tensor are derived to describe the magnetic response of the array and its dependence upon microwave frequency and external magnetic field. The model accounts for the geometrical parameters and the static magnetic configuration of the array, as well as the shape and intrinsic properties of the wires. We incorporate the effect of the static and dynamic interwire dipolar interactions and obtain explicit expressions for the position and relative amplitude of the two ferromagnetic resonance peaks associated with the effective permeability of nonsaturated arrays. The two absorption peaks arise due to the presence of the up and down wire populations, which are predominantly excited by the right-handed and left-handed circularly polarized magnetic field components of the electromagnetic wave propagating inside the array. Excellent agreement is found between the model and experimental results obtained from *S*-parameter broadband microstrip line measurements. Small discrepancies when the array is magnetically unsaturated or when the peaks are close to each other are discussed and attributed to spatial variations of the local interaction field not accounted for by the present model.

DOI: 10.1103/PhysRevB.80.224402 PACS number(s): 75.75.+a, 76.50.+g, 75.30.Gw

I. INTRODUCTION

The electromagnetic response of interacting systems based on ferromagnetic nanostructured materials constitutes a problem of general scientific interest. From the possibility of developing left-handed materials in metallic magnetic granular composites[1] to recent advances in magnonic crystals,[2,3] several studies have been concerned with the modeling of the magnetization dynamics and gyrotropic permeability response of nonhomogeneous magnetic materials.[4–8] In particular, the microwave response of saturated arrays of interacting ferromagnetic metallic nanowires has been the focus of many ferromagnetic resonance (FMR) studies,[9–13] in part due to their promising potential for the development of novel and tunable microwave devices.[4,14–16] While their magnetic anisotropy and thus FMR response can be controlled by the choice of composition and geometrical parameters,[9–13] a general model for the complex gyromagnetic permeability tensor $\vec{\mu}_{\text{eff}}$ of ferromagnetic nanowire arrays, which accurately describes their dependence upon static field, frequency, geometrical parameters, dipolar interactions, and static magnetic configuration, is still needed to properly assess their technological potential and to design competitive devices.

Nanowires of high quality, compatible with microwave integrated circuits, can be fabricated using low-cost electrochemical processes.[17] They exhibit saturation magnetization values larger than that of conventional microwave ferrites, usually permitting higher operating frequencies. Their small diameters compared to the microwave skin depth and their dilution in a dielectric matrix help reduce the eddy current losses generally associated with the presence of bulk metals. The intrinsic shape anisotropy of elongated nanowires leads to arrays with high remanent magnetization and to the possibility of developing microwave devices operating without an external magnetic field.[18] Recently, Encinas *et al.*[19] showed that the FMR response of self-biased dilute arrays of bistable Co nanowires depends on the static magnetic configuration of the array, that is, the relative fractions of wires having their magnetization oriented parallel or antiparallel to the external axial magnetic field. They applied various demagnetizing cycles to prepare different remanent states, characterized by specific FMR properties, and introduced the idea of field-programmable microwave devices. Kou *et al.*[20] reported similar results in dense arrays of axially magnetized NiFe nanowires, in which the interwire dipolar interactions strongly affect the observed response. They showed that the zero-field FMR frequency can be tuned over a large dynamic range by varying the remanent state of the array. They presented an expression for the FMR frequency of the array based on Kittel's formula,[21] to which they added a correction term. This term is essentially the remanent magnetization of the array multiplied by a geometrical factor introduced to reflect the static interwire dipolar interaction field along the wire axis. However, their expression neglects the dynamic interwire dipolar interactions perpendicular to the wire axis and does not recover the relation expected for saturated arrays in the monopolar regime[9] [see also our Eq. (38)]. As for many other reports,[9–13,15] their approach is also limited to giving the position of the FMR and does not yield the effective gyrotropic permeability response of the nanowire array.

In a recent study, we have used broadband microstrip line measurements to investigate the frequency-dependent micro-

wave response of dense arrays of axially magnetized CoFeB nanowires embedded in a nanoporous alumina membrane.[22] Below saturation, we observed two FMR peaks associated with the presence of two oppositely magnetized wire populations. We made use of a model for the effective permeability tensor of the array, based on a Maxwell-Garnett formalism established previously for saturated arrays,[23] and extended to account for the presence of two interacting oppositely magnetized bistable wire populations. This theoretical result was then used to calculate the transmission coefficient of the microstrip line and to yield explicit expressions for the two FMR peaks. We found good agreement between the theoretical and experimental field dependences of the two FMR peaks, both in terms of frequency and relative amplitude. Here, we present the hypotheses underlying the model, obtain the effective permeability tensor for nonsaturated arrays of axially magnetized bistable ferromagnetic nanowires, and derive analytical expressions for the resonance frequencies. We validate the model by comparison with experimental results and provide a physical interpretation of the double FMR phenomenon.

The paper is structured as follows. The model formulation is presented in Sec. II. We use an extended Maxwell-Garnett homogenization procedure to derive the effective permeability tensor $\vec{\vec{\mu}}_{\text{eff}}$ for ferromagnetic nanowire arrays with two populations of oppositely magnetized bistable inclusions. The resulting compact expression [Eq. (11)] depends on the individual magnetization response of the up and down wires subjected to a local field including both the static and dynamic interwire dipolar interaction fields. Solving the equation of motion for the magnetization of the two populations yields explicit expressions for the diagonal and off-diagonal components of $\vec{\vec{\mu}}_{\text{eff}}$ [Eqs. (27) and (28)], which constitutes the main result of this work. We also present an eigenmode analysis of the effective magnetization response of the array and establish the general resonance conditions [Eq. (37)] for the two FMR peaks observed experimentally. The comparison between the theoretical model and experimental data obtained from *S*-parameter broadband microstrip line measurements is presented in Sec. III and discussed in Sec. IV. The agreement between the model and experimental results is excellent.

II. MODEL FORMULATION

A. Preliminary definitions

We consider an array of ferromagnetic nanowires of diameter $d=2a$, length $L \gg d$, interwire distance D, and saturation magnetization M_s, as shown in Fig. 1. The wires are embedded in the nanopores of a dielectric circular membrane and are distributed in a symmetrical network (hexagonal, square, or randomly distributed network of wires). They occupy a volume fraction assumed equal to the surface pore density $P \propto \pi a^2/D^2$ of the membrane. The wire axis defines the z axis of a Cartesian coordinate system xyz and coincides with the direction of the externally applied static magnetic field $\mathbf{H}_0=H_0\hat{\mathbf{z}}$. The z axis also determines the out-of-plane direction, whereas the x and y axes define the in-plane directions.

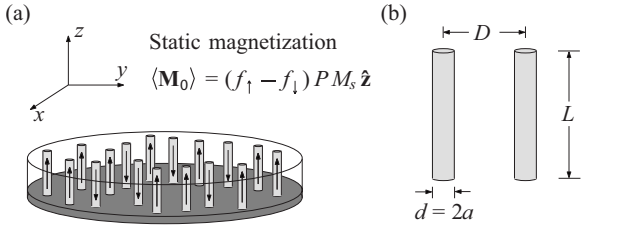

FIG. 1. (a) Schematic representation of a nonsaturated array of axially magnetized bistable ferromagnetic nanowires and definition of the Cartesian coordinate system xyz and average static magnetization of the array $\langle \mathbf{M}_0 \rangle$. (b) Definition of the geometrical parameters of the nanowires.

We model the individual wires as axially magnetized bistable single domains with static magnetization $\mathbf{M}_0 = \pm M_s\hat{\mathbf{z}}$. When the array is saturated, the wires all have their magnetization pointing in the same direction, such that the average static magnetization of the array is $\langle \mathbf{M}_0 \rangle = \pm PM_s\hat{\mathbf{z}} = \pm \langle M_{0s} \rangle \hat{\mathbf{z}}$, where the sign choice follows from that of H_0 and $\langle M_{0s} \rangle = PM_s$ is the saturation magnetization of the array. Below saturation, we have $|\langle \mathbf{M}_0 \rangle| = \langle M_0 \rangle < \langle M_{0s} \rangle$ and we assume that this reduction is caused by the magnetization reversal of some of the wires, resulting in a uniform random distribution of two oppositely magnetized wire populations with average magnetization

$$\langle \mathbf{M}_0 \rangle = (f_\uparrow - f_\downarrow) PM_s\hat{\mathbf{z}} = \Delta f PM_s\hat{\mathbf{z}} = \Delta PM_s\hat{\mathbf{z}}, \tag{1}$$

where $f_\uparrow$ and $f_\downarrow$ are the fractions of wires with their static magnetization aligned in the positive and negative z directions, with $f_\uparrow + f_\downarrow = 1$. The term $\Delta f = f_\uparrow - f_\downarrow$ corresponds to the normalized average magnetization of the array along the z axis. We also define $\Delta P = \Delta f P = P_\uparrow - P_\downarrow$, with $P_{\uparrow,\downarrow} = f_{\uparrow,\downarrow} P$. At positive and negative saturations, $\Delta f = \pm 1$, whereas at coercivity, $\Delta f = 0$ and the average magnetization $\langle \mathbf{M}_0 \rangle$ vanishes. At $H_0 = 0$, we have $\langle \mathbf{M}_0 \rangle = \langle M_{0r} \rangle \hat{\mathbf{z}}$, where $\langle M_{0r} \rangle$ is the remanent magnetization of the array. In such a case, $\Delta f = \langle M_{0r} \rangle / \langle M_{0s} \rangle$ defines the normalized remanent state of the array. We emphasize here that obtaining the dependence of the normalized average magnetization of the array upon the applied field, that is, $\Delta f(H_0)$, is not trivial and requires modeling the static hysteresis curve of the array, which is beyond the scope of this work. Hence, we shall determine $\Delta f(H_0)$ from static magnetometric measurements, then use it as a parameter in dynamic calculations at a given applied field H_0.

B. Maxwell-Garnett formalism

Our goal is to obtain the complex tensorial magnetic response of a nonsaturated array of axially magnetized bistable ferromagnetic nanowires subjected to an electromagnetic wave. When the length of the wave propagating within a composite material is much larger than the size and separation of the inclusions, the medium can be treated as homogeneous and be characterized by an effective dynamic permeability tensor $\vec{\vec{\mu}}_{\text{eff}}$, relating the average field and induction inside the medium,

$$\langle \mathbf{b} \rangle = \overleftrightarrow{\mu}_{\text{eff}} \langle \mathbf{h} \rangle, \tag{2}$$

where angular brackets and lower case letters denote spatially averaged and dynamic field quantities, respectively. Obtaining an expression for $\overleftrightarrow{\mu}_{\text{eff}}$ of a composite material usually requires one to consider effective medium theories.[24] In this context, various approaches have been proposed for modeling the permeability response of saturated ferromagnetic wire arrays.[4,7,23] In Ref. 23, we established a model for $\overleftrightarrow{\mu}_{\text{eff}}$ in the saturated regime based on a Maxwell-Garnett mixing rule valid for ellipsoidal inclusions with a gyrotropic permeability tensor and embedded in an isotropic nonmagnetic matrix. Here, we shall generalize this approach to nonsaturated arrays of axially magnetized bistable nanowires by extending our Maxwell-Garnett formalism to the case of two types of inclusions with antiparallel directions of static magnetization.

Let us consider the dynamic fields $\langle \mathbf{h} \rangle$ and $\langle \mathbf{b} \rangle$ entering Eq. (2) and decompose them,

$$\langle \mathbf{h} \rangle = P[f_{\uparrow} \langle \mathbf{h}_{w\uparrow} \rangle + f_{\downarrow} \langle \mathbf{h}_{w\downarrow} \rangle] + (1-P) \langle \mathbf{h}_m \rangle, \tag{3}$$

$$\langle \mathbf{b} \rangle = P[f_{\uparrow} \langle \mathbf{b}_{w\uparrow} \rangle + f_{\downarrow} \langle \mathbf{b}_{w\downarrow} \rangle] + (1-P) \langle \mathbf{b}_m \rangle, \tag{4}$$

where the subscripts m and w refer to average field quantities in the host matrix and wires, respectively. The average field and induction in the matrix can be assumed to be spatially uniform within a unit cell of the array, leading to

$$\langle \mathbf{h}_m \rangle = \mathbf{h}_{\text{loc}}, \tag{5}$$

$$\langle \mathbf{b}_m \rangle = \mu_0 \langle \mathbf{h}_m \rangle = \mu_0 \mathbf{h}_{\text{loc}}, \tag{6}$$

where $\mathbf{h}_{\text{loc}}$ is the dynamic local field in the matrix that excites the individual wires in the array and μ_0 is the permeability of free space. The local field on a given wire has contributions from the external field, due to sources located outside the sample (e.g., the microstrip line field), and from the sum of the dynamic dipolar interaction fields created by the dynamic magnetization of all the other wires in the array.

Now, consider $\langle \mathbf{h}_{w\uparrow,\downarrow} \rangle$ and $\langle \mathbf{b}_{w\uparrow,\downarrow} \rangle$ the average field and induction inside the up and down wire populations. In the regime of weak skin effect, usually valid for nanowires, the skin depth remains larger than the wire radius. In such a case, the magnetic field and induction are spatially uniform within the metallic wires and we can write

$$\langle \mathbf{h}_{w\uparrow,\downarrow} \rangle = \mathbf{h}_{w\uparrow,\downarrow}, \tag{7}$$

$$\langle \mathbf{b}_{w\uparrow,\downarrow} \rangle = \mu_0 (\mathbf{h}_{w\uparrow,\downarrow} + \mathbf{m}_{\uparrow,\downarrow}), \tag{8}$$

where $\mathbf{m}_{\uparrow,\downarrow}$ is the dynamic component of the up and down wire magnetizations. Next, we must express $\mathbf{h}_{w\uparrow,\downarrow}$ and $\mathbf{m}_{\uparrow,\downarrow}$ in terms of the local field $\mathbf{h}_{\text{loc}}$. Since uniform magnetization oscillations are excited inside the individual wires, modeled as elongated ellipsoids, it follows that[25]

$$\mathbf{h}_{w\uparrow,\downarrow} = \mathbf{h}_{\text{loc}} - \overleftrightarrow{N}_w \mathbf{m}_{\uparrow,\downarrow}, \tag{9}$$

$$\mathbf{m}_{\uparrow,\downarrow} = \overleftrightarrow{\eta}_{w\uparrow,\downarrow} \mathbf{h}_{\text{loc}}, \tag{10}$$

where $\overleftrightarrow{N}_w$ is the shape demagnetizing tensor of the individual wires and $\overleftrightarrow{\eta}_{w\uparrow,\downarrow}$ represents the wire external susceptibility tensor, which connects the wire magnetization response to the local field $\mathbf{h}_{\text{loc}}$. Substituting Eqs. (5)–(10) into Eqs. (2) and (4) leads to two equations for $\langle \mathbf{b} \rangle$ in terms of $\mathbf{h}_{\text{loc}}$. We equate these to yield a Maxwell-Garnett-like expression for the effective permeability tensor

$$\frac{\overleftrightarrow{\mu}_{\text{eff}}}{\mu_0} = \overleftrightarrow{I} + P[\overleftrightarrow{\eta}_w^{-1} - P\overleftrightarrow{N}_w]^{-1}, \tag{11}$$

where $\overleftrightarrow{I}$ is the identity matrix and

$$\overleftrightarrow{\eta}_w = f_{\uparrow} \overleftrightarrow{\eta}_{w\uparrow} + f_{\downarrow} \overleftrightarrow{\eta}_{w\downarrow} \tag{12}$$

is an equivalent external susceptibility tensor defined as the sum of the external responses of the two wire populations, weighted by their respective relative fraction. The introduction of $\overleftrightarrow{\eta}_w$ in Eq. (11) yields a relation for $\overleftrightarrow{\mu}_{\text{eff}}$ identical in form to the Maxwell-Garnett expression one would obtain in the case of composites with a single type of inclusions, such as saturated wire arrays.[23] To go further with Eq. (11), we must now establish expressions for the individual wire responses $\overleftrightarrow{\eta}_{w\uparrow}$ and $\overleftrightarrow{\eta}_{w\downarrow}$.

C. Response of an individual wire

Let us derive the dynamic magnetization response $\mathbf{m}_{\uparrow,\downarrow} = \overleftrightarrow{\eta}_{w\uparrow,\downarrow} \mathbf{h}_{\text{loc}}$ of the individual up and down wires in the array. Both populations experience the same local field $\mathbf{h}_{\text{loc}}$ oriented transverse to the wire axis. The dynamics of a wire with total magnetization

$$\mathbf{M}_{\uparrow,\downarrow} = \pm M_s \hat{\mathbf{z}} + \mathbf{m}_{\uparrow,\downarrow} \tag{13}$$

can be described by the Landau-Lifshitz-Gilbert equation of motion,

$$\frac{\partial \mathbf{M}_{\uparrow,\downarrow}}{\partial t} = -\mathbf{M}_{\uparrow,\downarrow} \times \left(\mu_0 |\gamma| \mathbf{H}_{w\uparrow,\downarrow} - \frac{\alpha}{M_s} \frac{\partial \mathbf{M}_{\uparrow,\downarrow}}{\partial t} \right), \tag{14}$$

where $-|\gamma| = -g\mu_B/\hbar$ is the gyromagnetic ratio, with g as the spectroscopic splitting factor, μ_B as the Bohr magneton, and $\hbar$ as the Planck constant divided by 2π, while α is the Gilbert phenomenological damping constant. The term $\mathbf{H}_{w\uparrow,\downarrow} = \mathbf{H}_{w0\uparrow,\downarrow} + \mathbf{h}_{w\uparrow,\downarrow}$ is the sum of the static and dynamic fields that act upon the magnetic moments inside each ferromagnetic wire. For long and axially magnetized wires, the static shape demagnetizing factor is essentially zero. Hence, the internal static field $\mathbf{H}_{w0\uparrow,\downarrow}$ inside a given wire in the array is the sum of the external field $\mathbf{H}_0$ and the interwire dipolar interaction field created by all the other wires of both populations. It is the same for the up and down wire populations and can be written as

$$\mathbf{H}_{w0\uparrow,\downarrow} = \mathbf{H}_{w0} = (H_0 - \Delta f N_{\text{op}}^{\text{int}} M_s) \hat{\mathbf{z}}. \tag{15}$$

Here, $N_{\text{op}}^{\text{int}}$ is the out-of-plane (axial) component of the interaction tensor introduced in Ref. 13 to model the angle-dependent FMR response of nanowire arrays in terms of an

effective demagnetizing factor including both intrawire and interwire dipolar interactions. It is given by

$$N_{\mathrm{op}}^{\mathrm{int}} = P\sum_{m=1}^{\infty} \frac{ms}{(m^2+s^2)^{3/2}}, \tag{16}$$

where $s=L/2D$ is a normalized length parameter. The sum in Eq. (16) depends on geometrical parameters only and tends asymptotically to unity in the monopolar regime, in which $L \gg D$. In such a case, $N_{\mathrm{op}}^{\mathrm{int}}$ reduces to P and Eq. (15) simplifies to

$$\mathbf{H}_{w0} = (H_0 - \Delta f P M_s)\hat{\mathbf{z}} = (H_0 - \Delta P M_s)\hat{\mathbf{z}}. \tag{17}$$

Depending on the sign of Δf, the static interwire interaction field will be either parallel or antiparallel to the z axis. The dynamic field within the wires is connected to the local field by Eq. (9), which becomes

$$\mathbf{h}_{w\uparrow,\downarrow} = \mathbf{h}_{\mathrm{loc}} - \tfrac{1}{2}\mathbf{m}_{\uparrow,\downarrow} \tag{18}$$

for long wires with transverse shape demagnetizing factors equal to 1/2. Using Eqs. (17) and (18), we can write

$$\mathbf{H}_{w\uparrow,\downarrow} = \mathbf{H}_{w0} + \mathbf{h}_{w\uparrow,\downarrow} = (H_0 - \Delta P M_s)\hat{\mathbf{z}} + \mathbf{h}_{\mathrm{loc}} - \tfrac{1}{2}\mathbf{m}_{\uparrow,\downarrow}. \tag{19}$$

Then, substituting Eq. (19), along with Eq. (13), into the small-signal limit of Eq. (14) and assuming a time dependence of the form $e^{-i\omega t}$ yield the linearized equations of motion for $\mathbf{m}_{\uparrow}$ and $\mathbf{m}_{\downarrow}$,

$$i\omega\mathbf{m}_{\uparrow} = \hat{\mathbf{z}} \times (\omega_M \mathbf{h}_{\mathrm{loc}} - \omega_{\uparrow}^{*}\mathbf{m}_{\uparrow}), \tag{20a}$$

$$-i\omega\mathbf{m}_{\downarrow} = \hat{\mathbf{z}} \times (\omega_M \mathbf{h}_{\mathrm{loc}} - \omega_{\downarrow}^{*}\mathbf{m}_{\downarrow}). \tag{20b}$$

In Eqs. (20a) and (20b), $\omega_M = \mu_0|\gamma|M_s$ and

$$\omega_{\uparrow,\downarrow}^{*} = \omega_{\uparrow,\downarrow} - i\alpha\omega = \left(\frac{\omega_M}{2} \pm \omega_H\right) - i\alpha\omega, \tag{21}$$

where

$$\omega_H = \mu_0|\gamma|(H_0 - \Delta P M_s) = \omega_0 - \Delta P \omega_M \tag{22}$$

is the static internal field expressed in units of angular frequency and $\omega_0 = \mu_0|\gamma|H_0$ is proportional to the applied static field. The upper and lower sign choices in Eq. (21) refer to the up and down wire populations, respectively. Solving Eqs. (20a) and (20b) for $\mathbf{m}_{\uparrow}$ and $\mathbf{m}_{\downarrow}$ in terms of $\mathbf{h}_{\mathrm{loc}}$ yields the external susceptibility tensor of the two wire populations,

$$\mathbf{m}_{\uparrow,\downarrow} = \overleftrightarrow{\eta}_{w\uparrow,\downarrow}\mathbf{h}_{\mathrm{loc}} = \begin{pmatrix} \eta_{\uparrow,\downarrow} & -i\eta_{t\uparrow,\downarrow} & 0 \\ i\eta_{t\uparrow,\downarrow} & \eta_{\uparrow,\downarrow} & 0 \\ 0 & 0 & 0 \end{pmatrix}\mathbf{h}_{\mathrm{loc}}, \tag{23}$$

with diagonal and off-diagonal components

$$\eta_{\uparrow,\downarrow} = \frac{\omega_M \omega_{\uparrow,\downarrow}^{*}}{(\omega_{\uparrow,\downarrow}^{*})^2 - \omega^2}, \quad \eta_{t\uparrow,\downarrow} = \pm\frac{\omega_M \omega}{(\omega_{\uparrow,\downarrow}^{*})^2 - \omega^2}. \tag{24}$$

The tensor $\overleftrightarrow{\eta}_{w\uparrow,\downarrow}$ describes how the wire magnetization $\mathbf{m}_{\uparrow,\downarrow}$ depends on frequency, internal static field, wire shape N_w, and intrinsic properties M_s, g, and α. The diagonal and off-diagonal components of $\overleftrightarrow{\eta}_{w\uparrow}$ and $\overleftrightarrow{\eta}_{w\downarrow}$ may then be substituted into Eq. (12) to yield the equivalent external susceptibility tensor $\overleftrightarrow{\eta}_{w}$, which accounts for the static magnetic configuration of the array, that is, the relative fractions $f_{\uparrow}$ and $f_{\downarrow}$ of up and down wires.

In the low-damping limit $\alpha \ll 1$, the FMR frequencies of the up and down populations in the *local* field $\mathbf{h}_{\mathrm{loc}}$ are thus given by $|\omega_{\uparrow}|$ and $|\omega_{\downarrow}|$, respectively. However, the two peaks observed experimentally are related to the effective permeability tensor $\overleftrightarrow{\mu}_{\mathrm{eff}}$, that is, to the response of the array in the *average* field $\langle\mathbf{h}\rangle$, which we shall consider in Sec. II D. The responses $\overleftrightarrow{\eta}_{w\uparrow,\downarrow}$ and $\overleftrightarrow{\mu}_{\mathrm{eff}}$, expressed in terms of the local and average fields, respectively, differ due to the dynamic interwire interactions connecting the precessions of $\mathbf{m}_{\uparrow}$ and $\mathbf{m}_{\downarrow}$. Indeed, incorporating Eqs. (5), (7), and (9) into Eq. (3), the relation between $\langle\mathbf{h}\rangle$ and $\mathbf{h}_{\mathrm{loc}}$ may be written as

$$\langle\mathbf{h}\rangle = \mathbf{h}_{\mathrm{loc}} - \overleftrightarrow{N}_w(P_{\uparrow}\mathbf{m}_{\uparrow} + P_{\downarrow}\mathbf{m}_{\downarrow}), \tag{25}$$

where the last terms of Eq. (25) represent the dynamic dipolar interaction fields exerted on an individual wire by all the other wires. This illustrates the coupling between the dynamic magnetizations $\mathbf{m}_{\uparrow}$ and $\mathbf{m}_{\downarrow}$ of the up and down wire populations since the response of a given wire of either population is affected by the dynamic magnetization of both populations. Note that this coupling is accounted for implicitly by the Maxwell-Garnett homogenization procedure.

D. Effective permeability tensor

We can now substitute our result for $\overleftrightarrow{\eta}_{w}$ into Eq. (11) to yield the effective permeability tensor

$$\overleftrightarrow{\mu}_{\mathrm{eff}} = \mu_0(\overleftrightarrow{I} + \overleftrightarrow{\chi}_{\mathrm{eff}}) = \begin{pmatrix} \mu_{\mathrm{eff}} & -i\mu_{\mathrm{eff},t} & 0 \\ i\mu_{\mathrm{eff},t} & \mu_{\mathrm{eff}} & 0 \\ 0 & 0 & \mu_0 \end{pmatrix}, \tag{26}$$

which takes the form of a gyrotropic tensor, with diagonal and off-diagonal components,

$$\frac{\mu_{\mathrm{eff}}}{\mu_0} = 1 + \chi_{\mathrm{eff}} = 1 + \omega_M \frac{P_{\uparrow}\omega_{\uparrow}^{*}[(\omega_{\downarrow}^{*})^2 - \omega^2] + P_{\downarrow}\omega_{\downarrow}^{*}[(\omega_{\uparrow}^{*})^2 - \omega^2] - \left(\frac{\omega_M}{2}\right)[(P_{\uparrow}\omega_{\downarrow}^{*} + P_{\downarrow}\omega_{\uparrow}^{*})^2 - (\Delta P\omega)^2]}{\Omega_{+}\Omega_{-}}, \tag{27}$$

$$\frac{\mu_{\mathrm{eff},t}}{\mu_0} = \chi_{\mathrm{eff},t} = \omega_M \omega \frac{P_\uparrow[(\omega_\downarrow^*)^2 - \omega^2] - P_\downarrow[(\omega_\uparrow^*)^2 - \omega^2]}{\Omega_+ \Omega_-}, \tag{28}$$

where χ_{eff} and $\chi_{\mathrm{eff},t}$ are the components of the effective susceptibility tensor $\overleftrightarrow{\chi}_{\mathrm{eff}}$. The terms Ω_+ and Ω_- in the denominator of μ_{eff} and $\mu_{\mathrm{eff},t}$ are given by

$$\Omega_\pm = \omega^2 \mp \omega\left(2\omega_H - \frac{\Delta P \omega_M}{2}\right) - \omega_\uparrow^* \omega_\downarrow^* + \frac{\omega_M}{2}(P_\uparrow \omega_\downarrow^* + P_\downarrow \omega_\uparrow^*). \tag{29}$$

Solving the quadratic equations $\Omega_+=0$ and $\Omega_-=0$ yields the two FMR frequencies $\omega_{\mathrm{res}+}$ and $\omega_{\mathrm{res}-}$ of the effective permeability tensor, which are derived below and given in Eq. (37).

Equations (27) and (28) for the diagonal and off-diagonal components of the effective permeability tensor constitute the main result of this work. They allow for the description of the gyromagnetic, complex, and dispersive magnetic response of nonsaturated arrays of axially magnetized bistable ferromagnetic nanowires. In particular, they enter the propagation constant that governs the interaction of electromagnetic waves with an array placed in a transmission line.

E. Eigenmode analysis

The effective permeability tensor has the gyrotropic form of Eq. (26) in rectangular coordinates, that is, when the transverse average field and induction can be written in Cartesian coordinates as

$$\langle \mathbf{h} \rangle = \langle h_x \rangle \hat{\mathbf{x}} + \langle h_y \rangle \hat{\mathbf{y}}, \tag{30}$$

$$\langle \mathbf{b} \rangle = \langle b_x \rangle \hat{\mathbf{x}} + \langle b_y \rangle \hat{\mathbf{y}}. \tag{31}$$

In this linear basis, the diagonal and off-diagonal components of $\overleftrightarrow{\mu}_{\mathrm{eff}}$ are given by Eqs. (27) and (28). Each always displays two distinct FMR peaks at $\omega_{\mathrm{res}+}$ and $\omega_{\mathrm{res}-}$ [except where the peaks coincide; see Eq. (42) below].

It is of interest to obtain the eigenmodes corresponding to each of the two eigenfrequencies, as well as the single-peak effective scalar permeability associated with each of the two eigenmodes. It is straightforward to show that the effective permeability tensor becomes diagonal in the circular basis with right-handed circularly polarized (RHCP) and left-handed circularly polarized (LHCP) components.[25] Hence, we can write

$$\langle \mathbf{b} \rangle = \begin{pmatrix} \langle b_+ \rangle \\ \langle b_- \rangle \end{pmatrix} = \begin{pmatrix} \mu_{\mathrm{eff}+} & 0 \\ 0 & \mu_{\mathrm{eff}-} \end{pmatrix} \begin{pmatrix} \langle h_+ \rangle \\ \langle h_- \rangle \end{pmatrix}, \tag{32}$$

where $\langle h_\pm \rangle = \langle h_x \rangle \mp i \langle h_y \rangle$ and $\langle b_\pm \rangle = \langle b_x \rangle \mp i \langle b_y \rangle$, such that the upper and lower signs refer to the RHCP and LHCP modes, respectively. Note that in Eq. (32), we have not considered the nonmagnetic dynamic response $\langle b_z \rangle = \mu_0 \langle h_z \rangle$ along the wire axis. The components of $\overleftrightarrow{\mu}_{\mathrm{eff}}$ correspond to the circular effective permeability components $\mu_{\mathrm{eff}+}$ and $\mu_{\mathrm{eff}-}$, expressed in terms of the diagonal and off-diagonal components as

$$\mu_{\mathrm{eff}\pm} = \mu_{\mathrm{eff}} \pm \mu_{\mathrm{eff},t}, \tag{33}$$

from which it follows that

$$\mu_{\mathrm{eff}} = \frac{\mu_{\mathrm{eff}+} + \mu_{\mathrm{eff}-}}{2}, \quad \mu_{\mathrm{eff},t} = \frac{\mu_{\mathrm{eff}+} - \mu_{\mathrm{eff}-}}{2}. \tag{34}$$

Using Eqs. (27) and (28), we may derive explicit expressions for the circular components

$$\frac{\mu_{\mathrm{eff}\pm}}{\mu_0} = 1 - \omega_M \frac{P_\uparrow(\omega_\downarrow^* \pm \omega) + P_\downarrow(\omega_\uparrow^* \mp \omega)}{\Omega_\pm}. \tag{35}$$

Equation (35) indicates that the eigenfrequency $\omega_{\mathrm{res}+}$, satisfying $\Omega_+=0$, corresponds to a RHCP eigenmode with scalar effective permeability $\mu_{\mathrm{eff}+}$, whereas the eigenfrequency $\omega_{\mathrm{res}-}$, satisfying $\Omega_-=0$, refers to a LHCP eigenmode with scalar effective permeability $\mu_{\mathrm{eff}-}$. Hence, the circular effective permeability components $\mu_{\mathrm{eff}+}$ and $\mu_{\mathrm{eff}-}$ display each a single FMR peak, the position of which is given by $\omega_{\mathrm{res}+}$ and $\omega_{\mathrm{res}-}$, respectively.

From Eq. (35), we also note that $\mu_{\mathrm{eff}+}$ and $\mu_{\mathrm{eff}-}$ both possess a term proportional to $P_\uparrow$ and one proportional to $P_\downarrow$. These represent the contributions from the up and down wire populations to each of the circular effective permeability components. As such, we can write $\mu_{\mathrm{eff}\pm} = \mu_{\mathrm{eff}\pm\uparrow} + \mu_{\mathrm{eff}\pm\downarrow}$. Direct calculations show that near $\omega_{\mathrm{res}+}$, the contribution of the up wire population to the RHCP permeability $\mu_{\mathrm{eff}+}$ dominates that of the down population. Therefore, we find that $\mu_{\mathrm{eff}+} \simeq \mu_{\mathrm{eff}+\uparrow}$ and $|\mathbf{m}_\uparrow| \gg |\mathbf{m}_\downarrow|$. On the contrary, around $\omega_{\mathrm{res}-}$, it is the contribution of the down wire population that dominates the LHCP permeability $\mu_{\mathrm{eff}-}$, such that $\mu_{\mathrm{eff}-} \simeq \mu_{\mathrm{eff}-\downarrow}$ and $|\mathbf{m}_\uparrow| \ll |\mathbf{m}_\downarrow|$. Under these assumptions, Eqs. (27) and (34) for μ_{eff} may be simplified and expressed in the compact form,

$$\frac{\mu_{\mathrm{eff}}}{\mu_0} \simeq \frac{\mu_{\mathrm{eff}+\uparrow} + \mu_{\mathrm{eff}-\downarrow}}{2\mu_0} = 1 - \frac{\omega_M}{2}\left[\frac{P_\uparrow(\omega_\downarrow^* + \omega)}{\Omega_+} + \frac{P_\downarrow(\omega_\uparrow^* + \omega)}{\Omega_-}\right], \tag{36}$$

in which the conditions $\Omega_+=0$ at $\omega_{\mathrm{res}+}$ and $\Omega_-=0$ at $\omega_{\mathrm{res}-}$ now correspond exclusively to the resonance of the up and down wire populations, respectively.

F. Resonance conditions

In the low-damping limit, we may replace $\omega_{\uparrow,\downarrow}^*$ by $\omega_{\uparrow,\downarrow}$ in Eq. (29). Solving the two resulting quadratic equations $\Omega_+=0$ and $\Omega_-=0$ for ω leads to two positive solutions, $\omega_{\mathrm{res}+}$ and $\omega_{\mathrm{res}-}$, corresponding to the FMR frequencies of the effective permeability tensor $\overleftrightarrow{\mu}_{\mathrm{eff}}$. We find

$$\omega_{\mathrm{res}\pm} = \frac{\omega_M}{2}\left\{\left[1 - P + \left(\frac{\Delta P}{2}\right)^2\right]^{1/2} \mp \frac{\Delta P}{2}\right\} \pm \omega_H. \tag{37}$$

The frequencies $\omega_{\mathrm{res}\pm}$ yield the positions of the two FMR absorption peaks observed experimentally in nonsaturated arrays of axially magnetized bistable ferromagnetic nanowires. Hence, for specified values of H_0, Δf, geometrical parameters, and intrinsic properties, the model predicts both the positions and relative amplitudes of the two FMR peaks.

At saturation, we have $\Delta f = \pm 1$ and Eq. (37) simplifies, as expected, to the result obtained in Ref. 9, valid in the monopolar regime,

$$\omega_{\mathrm{res}\pm} = \pm\,\omega_0 + \frac{\omega_M}{2}(1-3P). \tag{38}$$

For unsaturated arrays, $|\Delta f|<1$ and we have two resonance conditions, such that Eq. (37) can be conveniently expressed as

$$\omega_{\mathrm{res}\pm} = \bar{\omega}_{\mathrm{res}} \pm \frac{\Delta\omega_{\mathrm{res}}}{2}, \tag{39}$$

where

$$\bar{\omega}_{\mathrm{res}} = \frac{\omega_M}{2}\left[\left(1-\frac{P}{2}\right)^2 - P_\uparrow P_\downarrow\right]^{1/2}, \tag{40}$$

$$\Delta\omega_{\mathrm{res}} = 2\left[\omega_0 - \left(\frac{5\Delta P}{4}\right)\omega_M\right] \tag{41}$$

represent the average and separation of the two FMR frequencies $\omega_{\mathrm{res}+}$ and $\omega_{\mathrm{res}-}$, respectively. Note that we have used $(\Delta P)^2=P^2-4P_\uparrow P_\downarrow$ in Eq. (37) to yield $\bar{\omega}_{\mathrm{res}}$ in the form of Eq. (40). The peaks merge at $\Delta\omega_{\mathrm{res}}=0$, corresponding to an applied field

$$H_0 = \left(\frac{5\Delta P}{4}\right)M_s = \left(\frac{5\langle M_{0s}\rangle}{4}\right)\Delta f. \tag{42}$$

We stress that Eq. (42) constitutes an implicit condition on the applied magnetic field since Δf depends nontrivially on H_0, as illustrated by the hysteresis curve $\Delta f(H_0)$ in Fig. 3 below. At remanence, the array is self-biased and the applied static field $H_0=0$, such that $\Delta\omega_{\mathrm{res}}=-5\Delta P\omega_M/2$. Equation (39) thus becomes

$$\omega_{\mathrm{res}\pm} = \bar{\omega}_{\mathrm{res}} \mp \left(\frac{5\Delta P}{4}\right)\omega_M. \tag{43}$$

In this case, the separation between the two peaks is proportional to $\Delta P=\Delta f P$ and thus varies linearly with the remanent state of the array Δf, which can be configured following minor hysteresis cycles.

In order to get more insights into the various fields contributing to the FMR frequencies, we perform a second-order series expansion in P of Eq. (37). This yields

$$\omega_{\mathrm{res}\pm} \simeq \frac{\omega_M}{2}\left(1 - P_{\uparrow,\downarrow} - \frac{P_\uparrow P_\downarrow}{2}\right) \pm (\omega_0 - \Delta P\omega_M), \tag{44}$$

where we have used $P_{\uparrow,\downarrow}=(P\pm\Delta P)/2$. In Eq. (44), the terms within the first and second pairs of parentheses describe the dynamic and static field contributions to the FMR frequencies, respectively. First, the three transverse dynamic terms include the shape demagnetizing field of the individual wires $\omega_M/2$, as well as two interwire dipolar fields. These correspond to the interaction of each resonant wire at $\omega_{\mathrm{res}\pm}$ with the dipolar fields produced by the populations of resonant ($\propto P_{\uparrow,\downarrow}$) and nonresonant ($\propto P_\uparrow P_\downarrow$) wires. Second, the static fields comprise the applied field $\pm\omega_0$, as well as the axial dipolar interaction field $\mp\Delta P\omega_M$ due to the two oppositely magnetized wire populations.

In most relevant cases, however, the dynamic interaction *between* the resonant and nonresonant populations, proportional to $P_\uparrow P_\downarrow \le P^2/4$, remains small. Therefore, a first-order series expansion in P of Eq. (37) is usually sufficient and leads to the simple approximate relation

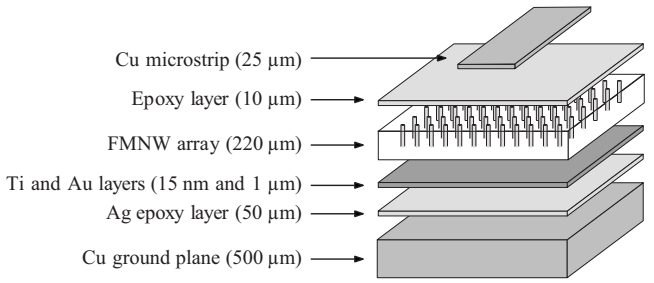

FIG. 2. Exploded view of the microstrip line deposited on the CoFeB ferromagnetic nanowire (FMNW) array.

$$\omega_{\mathrm{res}\pm} \simeq \frac{\omega_M}{2}(1-P_{\uparrow,\downarrow}) \pm \omega_H. \tag{45}$$

Physically, Eq. (45) is the limit of Eq. (37) when the small dynamic dipolar interaction between the up and down populations, proportional to $P_\uparrow P_\downarrow$ in Eq. (44), becomes negligible. This condition is usually fulfilled in nanowire arrays with P appreciably smaller than unity. In this approximation, the precessions of $\mathbf{m}_\uparrow$ and $\mathbf{m}_\downarrow$ are independent of each other and Eq. (36) for μ_{eff} applies. This assumes that the FMR peak observed in the effective permeability at $\omega_{\mathrm{res}+}$ ($\omega_{\mathrm{res}-}$) is due *solely* to the resonance of the magnetization $\mathbf{m}_\uparrow$ ($\mathbf{m}_\downarrow$) of the up (down) wire population. At remanence, Eq. (45) becomes

$$\omega_{\mathrm{res}\pm} \simeq \frac{\omega_M}{2}\left[1 - P\frac{(1\pm 5\Delta f)}{2}\right], \tag{46}$$

which depends linearly upon the remanent state Δf.

Finally, we note that the resonance conditions at remanence given in Eq. (4) in Ref. 20 can be obtained from Eq. (44) by setting $\omega_0=0$ and assuming that the second and third dynamic terms in the first pair of parentheses vanish. Their approach thus implicitly neglects the transverse dynamic dipolar interactions, both *within* the resonant and *between* the resonant and nonresonant wire populations. Moreover, it does not recover Eq. (38) at saturation.

III. COMPARISON WITH EXPERIMENT

A. Experimental procedure

We consider the comparison between the predictions of the model and experiment, expanding on the results presented in Ref. 22. An exploded view of the microstrip line structure on which measurements were performed is shown in Fig. 2. A two-step anodization procedure[26,27] was used for the fabrication of nanoporous alumina membranes. Scanning electron microscopy images of the alumina surface revealed a quasihexagonal ordering of the pores, with average pore diameter $d=45$ nm and average interpore distance $D=110$ nm. A 15-nm-thick Ti adhesion layer and a 1-μm-thick Au layer were successively sputtered onto one side of the alumina membrane prior to the electrodeposition of the nanowires. The Au layer served as a cathode in the

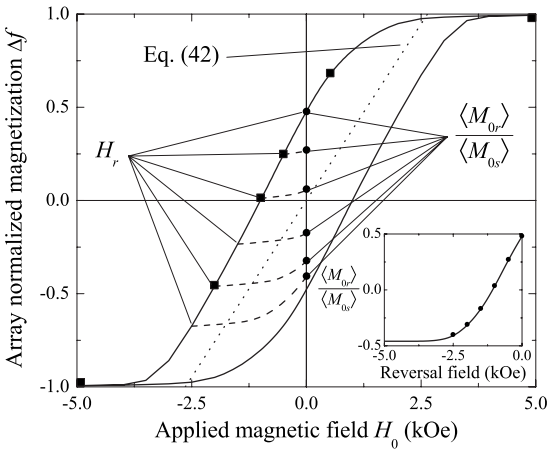

FIG. 3. Major hysteresis curve (solid line) of the normalized magnetization component $\Delta f=\langle M_0\rangle/\langle M_{0s}\rangle$ measured parallel to the static magnetic field H_0 applied along the nanowire axis. The dashed lines represent minor hysteresis curves measured for several reversal fields H_r, yielding states with different normalized remanent magnetization $\Delta f=\langle M_{0r}\rangle/\langle M_{0s}\rangle$. The squares and circles indicate the magnetic configurations corresponding to the permeability spectra shown in Figs. 4 and 6, respectively. The dotted line corresponds to the merging condition of the peaks [Eq. (42)], calculated using $M_s=1400$ kA/m and $P=0.12$. The inset shows the dependence of the normalized remanent magnetization of the array $\langle M_{0r}\rangle/\langle M_{0s}\rangle$ upon the reversal field H_r. Note that 1 kOe$=1000/4\pi\simeq 79.58$ kA/m in SI units.

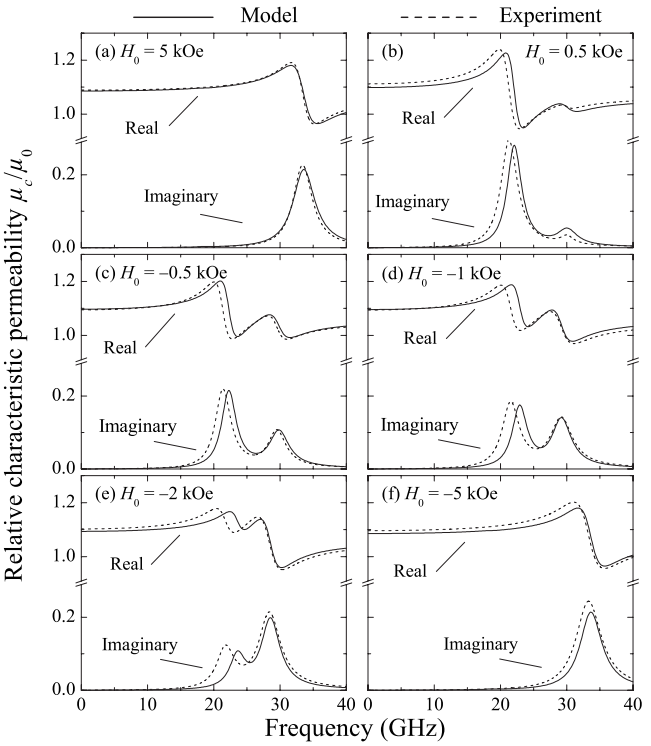

FIG. 4. Real and imaginary parts of the relative characteristic permeability μ_c/μ_0 as a function of frequency for CoFeB nanowires at several points $(H_0, \Delta f)$ along the upper branch of the major hysteresis curve, indicated by the squares in Fig. 3. (a) (5, 0.99), (b) (0.5, 0.67), (c) (−0.5, 0.25), (d) (−1, 0.001), (e) (−2, −0.46), and (f) (−5, −0.99). Dashed lines are experimental data extracted from the measured S parameters. Solid lines correspond to theoretical calculations using Eq. (47) with $q=0.13$ and μ_{eff} given by Eq. (27), with the following parameters: $M_s=1400$ kA/m, $g=2.26$, $\alpha=0.06$, and $P=0.12$. Note that 1 kOe$=1000/4\pi\simeq 79.58$ kA/m in SI units.

electrodeposition process and was later glued using Ag epoxy to the 500-μm-thick Cu ground plane of the microstrip line. Then, 220-μm-long amorphous $Co_{94}Fe_5B_1$ nanowires were electrodeposited inside the pores of the alumina membrane.[13] Finally, a standard lithography process was used to obtain a 0.5-mm-wide and 16-mm-long microstrip line on top of the CoFeB ferromagnetic nanowire array. A coaxial-to-microstrip line transition was used to connect a vector network analyzer to the microstrip line. Adjusting the width of the microstrip for impedance matching is not critical in this work, as we are mainly interested in extracting the intrinsic permeability of the nanowire array, in order to compare it with our theoretical model.

We used a vibrating sample magnetometer to obtain vectorial hysteresis curves for an array of CoFeB nanowires taken from the same membrane used to fabricate the microstrip line. Figure 3 shows the normalized magnetization component $\Delta f=\langle M_0\rangle/\langle M_{0s}\rangle$ (solid curve), measured parallel to the static magnetic field H_0 applied along the nanowire axis. For all measurements, the component of the magnetization perpendicular to the applied field is negligible, consistent with the assumption of two oppositely magnetized wire populations. Following minor hysteresis loops, it is possible to adjust the zero-field value of $\Delta f=\langle M_{0r}\rangle/\langle M_{0s}\rangle$ and hence to prepare specific remanent states. Figure 3 displays six minor hysteresis cycles, indicated by dashed lines, starting at reversal fields H_r ranging from −2.5 to 0 kOe, in steps of 0.5 kOe. The squares and circles indicate the magnetic configurations corresponding to the permeability spectra shown in Figs. 4 and 6, respectively. The dotted line corresponds to the merging condition of the peaks [Eq. (42)]. It is calculated using $M_s=1400$ kA/m and $P=0.12$ as parameter values, and it crosses the upper branch of the major hysteresis curve at $H_0\simeq 2.6$ kOe and $\Delta f\simeq 1$. The inset of Fig. 3 shows the behavior of the normalized remanence $\Delta f=\langle M_{0r}\rangle/\langle M_{0s}\rangle$ as a function of the reversal field H_r.

Broadband microstrip line measurements were performed in order to confront our effective permeability model against experimental data. We measured the S_{11} reflection and S_{21} transmission parameters of the microstrip line as a function of frequency (1–40 GHz) for different values of the static magnetic field H_0. The amplitude of the S_{21} parameter accounts for the transmission losses in the structure and is directly related to the FMR power absorption (a minimum in the transmission corresponds to a maximum in the absorption). In Ref. 22, we showed contour plots of the S_{21} parameter as a function of frequency and static magnetic field for both major and minor hysteresis cycles. Further, the levels of return loss and input impedance mismatch, described by the S_{11} parameter and reported in a previous study,[28] were not specifically adjusted to yield an optimally matched design with given characteristic impedance. Again, this does not constitute a significant concern in this work since we primarily focus on validating our formalism for the effective permeability tensor.

We assume that the microstrip line operates in the quasi-transverse electromagnetic (quasi-TEM) dominant mode of propagation, with dynamic electric and magnetic fields oriented respectively parallel and perpendicular to the nanowire wire axis. Hence, the wave propagates transverse to the average static magnetization of the array. In the case of an *unbounded* medium, the scalar permeability that characterizes wave propagation in this configuration is the Voigt permeability $\mu_{\text{eff}\perp}=(\mu_{\text{eff}}^2-\mu_{\text{eff},t}^2)/\mu_{\text{eff}}$. However, for *guided* waves propagating in a microstrip line structure, as considered in this work, it is the diagonal component μ_{eff} [Eq. (27)] that controls the propagation constant and that must be compared with the experimental permeability extracted from the measured S parameters.[29,30]

We used a numerical procedure similar to the transmission/reflection optimization method presented by Baker-Jarvis *et al.*[31] to extract, from the measured S parameters, experimental values of μ_c and ϵ_c. These correspond to the complex scalar *characteristic* permeability and permittivity of the entire microstrip line, which enter the definition for the characteristic impedance $Z_c=\sqrt{\mu_c/\epsilon_c}$ and propagation constant $k_c=\omega\sqrt{\mu_c\epsilon_c}$ of the structure in the quasi-TEM mode.[32] In Ref. 31, truncated Laurent series expansions are used to extract μ_c and ϵ_c. Here, we assume instead a double-peak Lorentzian resonant response for μ_c and a complex nondispersive response for ϵ_c.

The characteristic permeability μ_c is related to the effective permeability μ_{eff} of the nanowire array, as well as to the geometrical parameters of the microstrip line. Due to fringing-field effects, we find that μ_c is reduced compared to μ_{eff}. Expressions relating μ_c to μ_{eff}, based on a microwave magnetic filling factor, have been proposed by Pucel and Massé,[33] but they require that the permeability of the substrate be isotropic, with a strictly positive real part. Moreover, in our case, the presence of the 10-μm-thick low-permittivity epoxy layer between the Cu conducting strip and the nanowire array (see Fig. 2) increases the fringing fields in the structure, leading to a significant reduction of the apparent μ_c compared to the actual value of μ_{eff}.

From the above considerations, an *a priori* unknown factor, related to the geometrical and material parameters of the device under test, is expected to modify the calculated μ_{eff}. We have found that the experimental spectra for μ_c are well described by Eq. (27) for $\mu_{\text{eff}}=\mu_0(1+\chi_{\text{eff}})$, provided we use the following empirical relation, in the form proposed by Dionne and Oates,[34]

$$\mu_c=\mu_0(1+q\chi_{\text{eff}})=\mu_0+q(\mu_{\text{eff}}-\mu_0), \tag{47}$$

where q is a geometrical filling factor determined experimentally. It is equivalent to diluting the effective magnetic susceptibility response of the array χ_{eff}, due to its incorporation into the microstrip line structure. As shown below, a single value, $q=0.13$, enabled us to fit all of our data, without any further adjustment. The modeling of this q factor as a function of the microstrip line geometrical parameters lies, however, outside the scope of the present study.

B. Double ferromagnetic resonance

Let us first consider the permeability spectra as the applied field H_0 is swept from 5 down to −5 kOe, along the upper branch of the major hysteresis curve. Figure 4 displays the real and imaginary parts of the relative characteristic permeability μ_c/μ_0 as a function of frequency for the six applied magnetic fields indicated by the squares in Fig. 3. The spectra cover magnetic states extending from positive to negative saturation. The dashed lines correspond to the characteristic permeability extracted from the measured S parameters. The solid lines show the theoretical characteristic permeability calculated using Eq. (47) with $q=0.13$ and μ_{eff} given by Eq. (27), with the following experimentally determined parameters: $M_s=1400$ kA/m, $g=2.26$, $\alpha=0.06$, and $P=0.12$. We emphasize that this single set of parameter values was used to yield all the theoretical results presented in this work.

The model accounts fairly well for the position, shape, width, and amplitude of the two-peak permeability spectra obtained at different applied fields H_0 and associated static magnetic configurations Δf. The agreement is particularly good at saturation, where the permeability displays a single-peak resonant response [Figs. 4(a) and 4(f)], as well as for nonsaturated states characterized by two distinct well-separated peaks of substantially different amplitudes [Figs. 4(b) and 4(c)]. However, some discrepancies are observed in the permeability spectra exhibiting two relatively close peaks of similar amplitudes [Figs. 4(d) and 4(e)]. For these cases, corresponding to a situation where the number of down wires starts to exceed the number of up wires, the model tends to overestimate the resonance frequency of the peak at lower frequency and thus to underestimate the peak separation observed experimentally.

C. Dipolar interactions

The complete field dependence of the two FMR frequencies $\omega_{\text{res}+}$ and $\omega_{\text{res}-}$ is shown in Fig. 5 for the same down magnetic field sweep of the upper branch of the major hysteresis loop. Experimental data and theoretical calculations using Eq. (37) are denoted by squares and solid lines, respectively. The dashed portions of the curves indicate field intervals where only a single peak is observed (above 1 kOe and below −2.5 kOe). These correspond roughly to static magnetic configurations with $|\Delta f|\gtrsim 0.75$, for which one of the two populations is too dilute to exhibit a peak of significant intensity. As shown in the figure, the overall behavior is generally well accounted for by Eq. (37).

The field dependence of the two FMR peaks has been discussed previously[22] based on the behavior of the dipolar interaction field acting on each wire population as a function of $\Delta f(H_0)$. At applied fields above 1 kOe and below −2.5 kOe, the array is essentially saturated. Equation (38) then yields the FMR frequency of the single-peak effective permeability, which depends linearly on the applied field, in agreement with the experimental results shown in Fig. 5. As the applied field is decreased along the upper branch of the major hysteresis curve, the wires gradually reverse their magnetization, which in turn modifies the effective dynamic

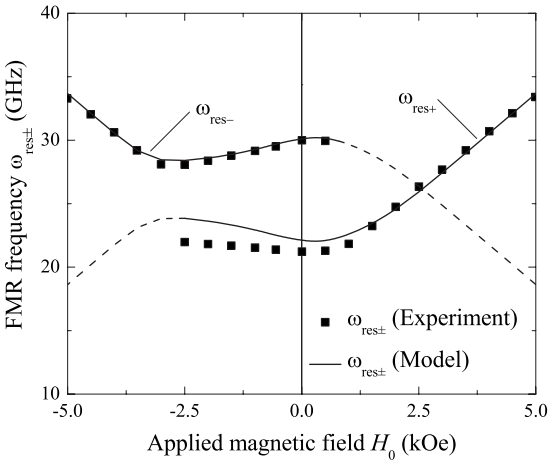

FIG. 5. Measured resonance frequencies ω_{res+} and ω_{res-} as a function of the decreasing applied magnetic field H_0 along the upper branch of the major hysteresis curve for CoFeB nanowires. The solid lines represent calculations of ω_{res+} and ω_{res-} using Eq. (37) with $M_s=1400$ kA/m, $g=2.26$, and $P=0.12$. The dashed portion of each curve indicates the field range where the amplitude of the peak at $\omega_{res\pm}$ is negligible compared to that of the peak at $\omega_{res\mp}$. This corresponds roughly to static magnetic configurations with $|\Delta f| \gtrsim 0.75$. Note that 1 kOe$=1000/4\pi \simeq 79.58$ kA/m in SI units.

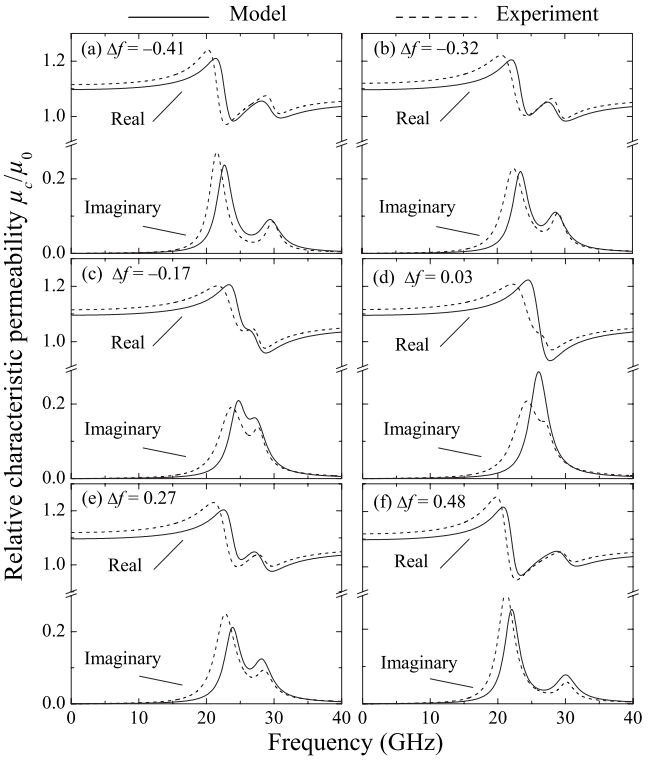

FIG. 6. Real and imaginary parts of the relative characteristic permeability μ_c/μ_0 as a function of frequency for CoFeB nanowires at several remanent states (H_r, Δf), indicated by the circles in Fig. 3. (a) (−2.5, −0.41), (b) (−2, −0.32), (c) (−1.5, −0.17), (d) (−1, 0.03), (e) (−0.5, 0.27), and (f) (0,0.48). Dashed lines are experimental data extracted from the measured S parameters. Solid lines correspond to theoretical calculations using Eq. (47) with $q=0.13$ and μ_{eff} given by Eq. (27), with $H_0=0$ and the following parameters: $M_s=1400$ kA/m, $g=2.26$, $\alpha=0.06$, and $P=0.12$. Note that 1 kOe$=1000/4\pi \simeq 79.58$ kA/m in SI units.

permeability of the array. In particular, as the nanowires begin to reverse randomly, the strength of the effective static dipolar interaction field, which is initially antiparallel to the magnetization of the up population, is gradually reduced. This produces the upward curvature observed in the resonance condition ω_{res+}. The second peak of smaller amplitude and higher frequency ω_{res-} becomes visible, beginning at about $H_0=0.5$ kOe. As the wires continue to reverse, the static interwire dipolar interaction increases parallel to the up and antiparallel to the down populations, yielding the opposite frequency behaviors of the two peaks with decreasing H_0, that is, ω_{res+} increases and ω_{res-} decreases. The two peaks come closer together until negative saturation is achieved at $H_0=-2.5$ kOe, below which the down population dominates the response and ω_{res-} becomes linear again with the applied field, as expected from Eq. (38).

As for the effective permeability spectra, the main discrepancies between the theoretical and experimental results for the FMR frequencies occur between −1 and −2.5 kOe, for which the model predicts a higher value for ω_{res+} than that observed experimentally. Although the extraction of μ_c from the measured S parameters is less reliable when the peaks are closer together and strongly convoluted, this is not likely to produce these systematic discrepancies apparently related to the reversal process. On the other hand, the precise positions of the resonance peaks during reversal could be quite sensitive to our hypothesis of an idealized array, characterized, during reversal, by two uniform distributions of up and down identical nanowire populations. Fluctuations of the uniform interaction field are expected to be more significant between coercive field, at $H_0=-1$ kOe, and the point of complete reversal of the wires, at $H_0=-2.5$ kOe. This aspect is developed further below, in relation to the results on remanent states.

D. Self-biased nanowire array

Let us now consider the dynamic response of the nanowire array in different remanent states described by $\Delta f=\langle M_{0r}\rangle/\langle M_{0s}\rangle$, as obtained from minor hysteresis curves. Figure 6 displays the real and imaginary parts of the relative characteristic permeability μ_c/μ_0 as a function of frequency, for $H_0=0$ and six values of reversal field H_r, ranging from −2.5 to 0 kOe, in steps of 0.5 kOe. These correspond to the minor loops displayed in Fig. 3 and to remanence values $\Delta f=\langle M_{0r}\rangle/\langle M_{0s}\rangle$ extending from −0.41 to 0.48, indicated by the circles in Fig. 3. Dashed lines correspond to the characteristic permeability extracted from the measured S parameters. Solid lines represent the theoretical characteristic permeability calculated using Eq. (47) with μ_{eff} given by Eq. (27). The model agrees very well with experimental results, except for small discrepancies at low remanence, where $|\Delta f| \ll 1$ and $f_\uparrow \simeq f_\downarrow$. This is illustrated in Fig. 6(d), where the theoretical permeability displays a single peak, whereas two peaks are observed experimentally.

This discrepancy near $|\Delta f|=0$ is further illustrated in Fig. 7, which compares the FMR frequencies obtained experimentally at remanence with the prediction of the model given by Eq. (43). The disagreement is higher for the low-

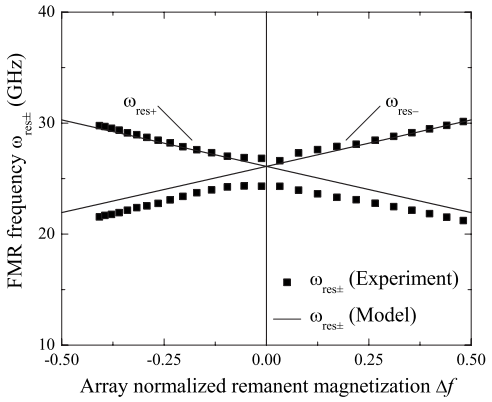

FIG. 7. Measured resonance frequencies $\omega_{\text{res+}}$ and $\omega_{\text{res-}}$ as a function of the normalized remanence of the array $\Delta f = \langle M_{0r} \rangle / \langle M_{0s} \rangle$ for CoFeB nanowires. The solid lines represent calculations of $\omega_{\text{res+}}$ and $\omega_{\text{res-}}$ as a function of Δf, using Eq. (43) with $M_s = 1400$ kA/m, $g = 2.26$, and $P = 0.12$. Note that 1 kOe $= 1000/4\pi \simeq 79.58$ kA/m in SI units.

frequency peak of the majority population, corresponding to the up wire population if $\Delta f > 0$ and down wire population if $\Delta f < 0$. At remanence, the majority population always exhibits, not surprisingly, a peak of higher amplitude and lower resonance frequency than the minority population since it experiences a stronger effective demagnetizing field originating in the interwire dipolar interactions. As for the saturated parts of the resonance conditions shown in Fig. 5, the slope and intercept of the linear behavior in Fig. 7 provide a useful mean of determining the saturation magnetization of the wires M_s and the porosity of the array P.

IV. DISCUSSION AND CONCLUSION

The general agreement between the model and experimental results shown in Figs. 4–7 demonstrates the capability of our model to describe and predict the complex dynamic permeability of ferromagnetic nanowire arrays placed in various static configurations as determined by H_0 and Δf. The model accounts well for the peak positions, as well as the line shapes and widths of both the real and imaginary parts of the permeability response, except for small disagreements in resonance positions when the peaks are close to each other. The difficulty, in such circumstances, is not related with the dynamic effective permeability model as such but most likely with our idealized assumption that the nanowires reverse in such a way as to constantly preserve a static magnetic configuration consisting of two oppositely magnetized and uniformly distributed wire populations described by a single parameter Δf.

Spatial fluctuations of the dipolar interactions, expected in real arrays, should modify their microwave response, particularly when the two resonance frequencies are close to each other or, equivalently, when the up and down populations experience the same average effective field. The condition $\Delta\omega_{\text{res}} = 0$, where the two peaks merge, would correspond to a straight line with a slope of $4/(5PM_s)$ and zero intercept on the normalized magnetization curve shown in Fig. 3. The merging condition is expected to be fulfilled when the line crosses a magnetization path, the upper branch of the major loop in our example. This condition is met at $H_0 \simeq 2.6$ kOe, as shown in Figs. 3 and 5. However, the merging is not observed experimentally, as it corresponds to a point $(H_0, \Delta f)$ located in the saturated portion of the hysteresis curve, where the effective permeability displays only a single peak.

The best condition to test our hypothesis of uniform interaction field is when the peaks merge in a globally demagnetized state $(\Delta f = 0)$, where the effective resonance field is due only to dipolar interactions. In Fig. 7, we have shown that minor magnetization cycles can bring the array to an almost perfectly demagnetized state. According to Eq. (43), $\omega_{\text{res+}}$ and $\omega_{\text{res-}}$ should coincide at $\omega_M(\sqrt{1-P})/2$ in such a demagnetized remanent state, which is not observed experimentally. The peaks remain well separated, suggesting a residual interaction between the up and down wire populations, even though the average static magnetization of the array nearly vanishes. This seems to provide further evidence of a local magnetization arrangement within the array, leading to a nonzero local interaction field along the wire axis and to different values of $\omega_{\text{res+}}$ and $\omega_{\text{res-}}$. Accounting for the experimental results in the region where the peaks are close to each other would require a model for the static hysteresis curve $\Delta f(H_0)$, which is considerably more involved and lies outside the scope of this work.

In summary, we have presented a model for the effective permeability tensor $\vec{\vec{\mu}}_{\text{eff}}$ of nonsaturated arrays of axially magnetized bistable ferromagnetic nanowires, based on a Maxwell-Garnett formalism generalized to include the case of two oppositely magnetized wire populations. We have established explicit expressions for the complex diagonal and off-diagonal components of the effective permeability tensor and have derived analytical expressions for the resonance frequencies. The model incorporates the effect of the static and dynamic dipolar interwire interactions, oriented parallel and transverse to the wire axis, respectively. In general, excellent agreement was found between the theory and experimental data obtained from broadband microstrip line measurements. The model could reproduce the complex permeability spectra extracted from the measured S parameters, both in terms of position, shape, width, and amplitude, as well as predict the dependence of the two FMR frequencies $\omega_{\text{res}\pm}$ upon applied magnetic field H_0 and normalized remanent magnetization Δf. The agreement is slightly reduced when the peaks are close to each other, suggesting a significant spatial variation of the local interaction field, which is not accounted for in the present model. Nevertheless, the proposed formalism yields valuable insights into the modeling of the effective dynamic response of composite materials with two types of interacting gyromagnetic inclusions and constitutes a step toward the understanding of the electromagnetic response of self-biased microwave devices based on ferromagnetic nanowire arrays.

ACKNOWLEDGMENTS

This work was supported by grants under NSERC (Canada) and FQRNT (Québec). The authors acknowledge Apollo Microwaves for financial support.

*vincent.boucher@polymtl.ca
†david.menard@polymtl.ca

[1] S. T. Chui and L. Hu, Phys. Rev. B **65**, 144407 (2002).
[2] M. Krawczyk and H. Puszkarski, Phys. Rev. B **77**, 054437 (2008).
[3] S. Neusser and D. Grundler, Adv. Mater. **21**, 2927 (2009).
[4] A. Saib, D. Vanhoenacker-Janvier, I. Huynen, A. Encinas, L. Piraux, E. Ferain, and R. Legras, Appl. Phys. Lett. **83**, 2378 (2003).
[5] R. Ramprasad, P. Zurcher, M. Petras, M. Miller, and P. Renaud, J. Appl. Phys. **96**, 519 (2004).
[6] V. B. Bregar, Phys. Rev. B **71**, 174418 (2005).
[7] J. Chen, D. Tang, B. Zhang, Y. Yang, M. Lu, H. Lu, F. Lu, and W. Xu, J. Appl. Phys. **102**, 023106 (2007).
[8] J. Ramprecht and D. Sjöberg, J. Phys. D **41**, 135005 (2008).
[9] A. Encinas-Oropesa, M. Demand, L. Piraux, I. Huynen, and U. Ebels, Phys. Rev. B **63**, 104415 (2001).
[10] M. Demand, A. Encinas-Oropesa, S. Kenane, U. Ebels, I. Huynen, and L. Piraux, J. Magn. Magn. Mater. **249**, 228 (2002).
[11] C. A. Ramos, E. Vassallo Brigneti, and M. Vázquez, Physica B **354**, 195 (2004).
[12] I. Dumitru, F. Li, J. B. Wiley, D. Cimpoesu, A. Stancu, and L. Spinu, IEEE Trans. Magn. **41**, 3361 (2005).
[13] L.-P. Carignan, C. Lacroix, A. Ouimet, M. Ciureanu, A. Yelon, and D. Ménard, J. Appl. Phys. **102**, 023905 (2007).
[14] A. Saib, M. Darques, L. Piraux, D. Vanhoenacker-Janvier, and I. Huynen, IEEE Trans. Microwave Theory Tech. **53**, 2043 (2005).
[15] B. Ye, F. Li, D. Cimpoesu, J. B. Wiley, J.-S. Jung, A. Stancu, and L. Spinu, J. Magn. Magn. Mater. **316**, e56 (2007).
[16] B. K. Kuanr, V. Veerakumar, R. L. Marson, S. R. Mishra, R. E. Camley, and Z. Celinski, Appl. Phys. Lett. **94**, 202505 (2009).
[17] A. Fert and L. Piraux, J. Magn. Magn. Mater. **200**, 338 (1999).
[18] A. Encinas, M. Demand, L. Vila, L. Piraux, and I. Huynen, Appl. Phys. Lett. **81**, 2032 (2002).
[19] A. Encinas, L. Vila, M. Darques, J. M. George, and L. Piraux, Nanotechnology **18**, 065705 (2007).
[20] X. Kou, X. Fan, H. Zhu, and J. Q. Xiao, Appl. Phys. Lett. **94**, 112509 (2009).
[21] C. Kittel, Phys. Rev. **73**, 155 (1948).
[22] L.-P. Carignan, V. Boucher, T. Kodera, C. Caloz, A. Yelon, and D. Ménard, Appl. Phys. Lett. **95**, 062504 (2009).
[23] V. Boucher and D. Ménard, J. Appl. Phys. **103**, 07E720 (2008).
[24] A. Sihvola, *Electromagnetic Mixing Formulas and Applications* (Institution of Electrical Engineers, London, 1999).
[25] A. G. Gurevich and G. A. Melkov, *Magnetization Oscillations and Waves* (CRC Press, Boca Raton, 1996).
[26] S. Zhao, K. Chan, A. Yelon, and T. Veres, Nanotechnology **18**, 245304 (2007).
[27] L.-P. Carignan, M. Massicotte, A. Yelon, C. Caloz, and D. Ménard, IEEE Trans. Magn. **45**, 4070 (2009).
[28] L.-P. Carignan, T. Kodera, A. Yelon, D. Ménard, and C. Caloz, *Proceedings of the 39th European Microwave Conference*, Rome (IEEE Press, Piscataway, NJ, 2009), pp. 743–746.
[29] M. Hines, IEEE Trans. Microwave Theory Tech. **19**, 442 (1971).
[30] E. Schloemann, J. Magn. Magn. Mater. **209**, 15 (2000).
[31] J. Baker-Jarvis, M. D. Janezic, J. H. Grosvenor, Jr., and R. G. Geyer, NIST Tech. Note **1355** (1992).
[32] L. F. Chen, C. K. Ong, C. P. Neo, V. V. Varadan, and V. K. Varadan, *Microwave Electronics: Measurement and Materials Characterization* (Wiley, New York, 2004).
[33] R. A. Pucel and D. J. Massé, IEEE Trans. Microwave Theory Tech. **20**, 304 (1972).
[34] G. F. Dionne and D. E. Oates, IEEE Trans. Magn. **33**, 3421 (1997).